

饱和吸收体恢复时间对正交偏振耗散孤子的影响

何晓颖 张川 张银东 饶岚

Influence of SA recovery time on orthogonally polarized dissipative solitons

HE Xiao-ying, ZHANG Chuan, ZHANG Yin-dong, RAO Lan

引用本文:

何晓颖, 张川, 张银东, 饶岚. 饱和吸收体恢复时间对正交偏振耗散孤子的影响[J]. *中国光学*, 2024, 17(3): 714–723. doi: 10.37188/CO.EN-2023-0032

HE Xiao-ying, ZHANG Chuan, ZHANG Yin-dong, RAO Lan. Influence of SA recovery time on orthogonally polarized dissipative solitons[J]. *Chinese Optics*, 2024, 17(3): 714–723. doi: 10.37188/CO.EN-2023-0032

在线阅读 View online: <https://doi.org/10.37188/CO.EN-2023-0032>

您可能感兴趣的其他文章

Articles you may be interested in

碲化铋倏逝场锁模器件的超快光纤激光器

Ultrafast fiber laser based on bismuth telluride evanescent field mode-locked device
中国光学 (中英文). 2022, 15(3): 433 <https://doi.org/10.37188/CO.2021-0216>

1.6 μm 波段锁模光纤激光器

1.6 μm band mode-locked fiber laser
中国光学 (中英文). 2021, 14(6): 1387 <https://doi.org/10.37188/CO.2021-0128>

偏振光在椭球细粒子中多次散射传输特性

Multiple scattering transmission characteristic of polarized light in ellipsoidal fine particles
中国光学 (中英文). 2023, 16(2): 348 <https://doi.org/10.37188/CO.2022-0144>

基于大气多次散射的波浪水下偏振模式研究

The polarization mode of underwater waves based on atmospheric multiple scattering
中国光学 (中英文). 2023, 16(6): 1324 <https://doi.org/10.37188/CO.2022-0223>

可提升被动锁模光纤激光器计算效率的分步傅里叶全局误差局部能量法

SSFM-global-error-local-energy method for improving computational efficiency of passively mode-locked fiber laser
中国光学 (中英文). 2023, 16(3): 733 <https://doi.org/10.37188/CO.EN.2022-0016>

正交激发发射上转换纳米材料的设计、制备与应用

Design, preparation and application of orthogonal excitation-emission upconversion nanomaterials
中国光学 (中英文). 2023, 16(1): 76 <https://doi.org/10.37188/CO.2022-0134>

文章编号 2097-1842(2024)03-0714-10

Influence of SA recovery time on orthogonally polarized dissipative solitons

HE Xiao-ying*, ZHANG Chuan, ZHANG Yin-dong, RAO Lan

(School of Electronic Engineering and Beijing Key Laboratory of Space-Ground Interconnection and Convergence, Beijing University of Posts and Telecommunications, Beijing 100876, China)

* Corresponding author, E-mail: xiaoyinghe@bupt.edu.cn

Abstract: Polarization is a crucial factor in shaping and stabilizing mode-locking pulses. We develop an orthogonally polarized numerical modeling of passive mode-locked graphene fiber lasers for generating orthogonally polarized dissipative solitons (DSs). The focus is on analyzing the influence of orthogonal polarization in this net-normal dispersion birefringent cavity caused by the polarization-dependent graphene microfiber saturable absorber. The research results demonstrate that the recovery time of such saturable absorbers significantly affects the characteristics of the orthogonally polarized DSs' output pulses, including energy, pulse width, time-bandwidth product, and chirps. Results show that its recovery time of 120 fs is optimal, producing two orthogonally polarized narrow dissipative soliton pulses with large chirps of about 7.47 ps and 8.06 ps. This has significant implications for the development of compact, high-power, polarized dissipative soliton fiber laser systems.

Key words: orthogonal polarization; passive mode-locking; net-normal dispersion; recovery time

饱和吸收体恢复时间对正交偏振耗散孤子的影响

何晓颖*, 张川, 张银东, 饶岚

(北京邮电大学电子工程学院 天地互联与融合北京市重点实验室, 北京 100876)

摘要: 偏振在脉冲锁模时, 对其塑形和稳定起着至关重要的作用。本研究开发了一种用于产生正交偏振耗散孤子的被动锁模石墨烯光纤激光器的正交偏振数值模拟。重点是分析由偏振依赖的石墨烯微光纤饱和吸收体引起的净正常色散双折射腔对正交偏振孤子的影响。研究表明, 这种饱和吸收体的恢复时间显著影响正交偏振耗散脉冲的特性, 如能量、脉宽、时间带宽乘积和啁啾。结果显示, 其恢复时间为120飞秒时最佳, 产生两个具有大啁啾的正交偏振的窄耗散孤子脉冲, 分别约为7.47 ps和8.06 ps。这对于开发紧凑、高功率、偏振耗散孤子光纤激光系统具有重要意义。

关键词: 正交偏振光; 被动锁模; 净正常色散腔; 恢复时间

中图分类号: O436.3

文献标志码: A

doi: 10.37188/CO.EN-2023-0032

收稿日期: 2023-12-15; 修订日期: 2024-01-04

基金项目: 国家自然科学基金(No. 61675046, No. 61935005)

Supported by National Natural Science Foundation of China (No. 61675046, No. 61935005)

1 Introduction

Passive mode-locked (PML) fiber lasers have attracted much attention because of their advantages of high stability, higher beam quality, and compact structure^[1-5]. In PML lasers, saturable absorbers (SAs) are often used as passive mode-locking elements, crucial in forming optical solitons^[6-14]. Graphene has been chosen as an ideal saturable absorber because of its unique characteristics, such as ultrafast carrier dynamics, wide spectral bandwidth, and high optical damage threshold^[15]. In 2010, Sun *et al.* demonstrated the graphene film as a saturable absorber in the fiber laser to generate mode-locked pulses^[16]. Polarization plays a crucial role in formatting and stabilizing mode-locking pulses. Moreover, polarization serves to suppress noises in PML fiber lasers. Orthogonally polarized light significantly influences coherence, energy distribution, and pulse characteristics in PML fiber lasers. Graphene has advantages over traditional SAs like semiconductor saturable absorption mirrors (SESAMs); for example, the flexibility to cover the optical waveguide, a wide wavelength absorption spectra, and ultrafast carrier relaxation time for easily generating and controlling orthogonal polarization dissipative solitons. Therefore, it is necessary to study the evolutionary behavior and the impact of orthogonally polarized states on PML fiber lasers with graphene saturable absorbers.

Various soliton states in the graphene PML fiber laser have been studied extensively^[17-19]. Conventional solitons (CS) were discovered in fiber lasers with net negative cavity dispersion to obtain a natural balance between cavity dispersion and fiber nonlinearity^[20]. Other solitons, such as dissipative solitons (DSs), have been formed in graphene PML fiber lasers operating in the regime of net-normal cavity dispersion^[21]. DSs are coherent solutions of nonlinear wave equations that require an intricate and mutual interaction of nonlinearity, dispersion,

loss, and gain^[22-24]. Their stable high-energy pulses make them ideal for high-energy laser machining^[25]. In 2021, by numerical simulations, Lee *et al.* demonstrated the optimal range of SA recovery time on the formation of dissipative solitons in Yb-doped fiber lasers^[26]. In 2022, Xu *et al.* achieved group-velocity-locked vector solitons switching between CS and DS by using a birefringent-related intracavity Lyot filter with an adjustable extinction ratio in the mode-locking fiber laser^[27]. However, in birefringent cavities, the effect of orthogonal polarization caused by polarization-dependent components on vector DS is hard to observe in intracavity and often overlooked. The vector DSs have significant potential for application in optics and quantum communication systems^[28].

In this paper, we build an orthogonally polarized numerical modeling of the graphene PML fiber laser with net-normal dispersion birefringent cavity for generating vector DSs. A polarization-dependent graphene saturable absorber is utilized to form a birefringent cavity. The effect of the recovery time of such polarization-dependent saturable absorbers on output DSs and optical spectra has been discussed and analyzed. This is of great significance for the development of vector DSs systems.

2 Numerical modeling

The schematic diagram of the graphene PML fiber laser is depicted in Fig. 1. The dispersion of the erbium-doped fiber (EDF) and single-mode fiber (SMF) employed in our laser are -46.25 ps/nm/km and 28 ps/nm/km, respectively, both possessing the same nonlinear coefficient of 0.004 W⁻¹·m⁻¹. An isolator (ISO) is implemented to enforce unidirectional operation within the fiber ring cavity. A 30:70 fiber optical coupler with a 30% port extracts the laser pulse output. Graphene is half-covered on the microfiber for polarization-dependent saturable absorber, called graphene half-covered microfiber SAs (GMSA). A bandpass filter with a bandwidth of

8 nm is utilized in our model to play a crucial role in the formation of DSs^[29]. A squeeze-typed polarization controller (PC) is employed to adjust the polarization state of pulses entering the GMSA. Due to the polarization-dependent property of the GMSA^[30], we first set the initial absorption rate of the saturable absorber (SA) to 0.56 for the X-polarization and 0.43 for the Y-polarization.

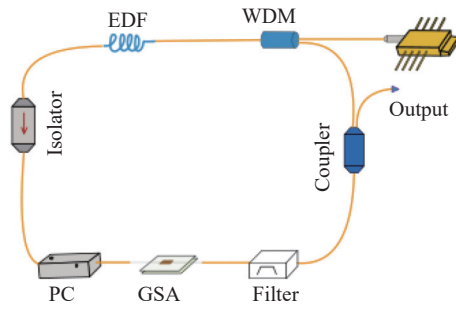


Fig. 1 Schematic diagram of polarization-locked mode-locked fiber laser

The total transmission $T(I)$ of a SA consists of

$$\begin{aligned} \frac{\partial u}{\partial z} &= -\frac{\alpha}{2}u - \delta \frac{\partial u}{\partial T} - i\frac{\beta_2}{2} \frac{\partial^2 u}{\partial T^2} + i\gamma \left(|u|^2 + \frac{2}{3}|v|^2 \right) u + \frac{g}{2}u + \frac{g}{2\Omega_g^2} \frac{\partial^2 u}{\partial T^2} \\ \frac{\partial v}{\partial z} &= -\frac{\alpha}{2}v - \delta \frac{\partial v}{\partial T} - i\frac{\beta_2}{2} \frac{\partial^2 v}{\partial T^2} + i\gamma \left(|v|^2 + \frac{2}{3}|u|^2 \right) v + \frac{g}{2}v + \frac{g}{2\Omega_g^2} \frac{\partial^2 v}{\partial T^2} \end{aligned} \quad (3)$$

where u and v represent the envelopes of the optical pulses along the two orthogonal polarization modes along the fiber, α is the loss coefficient of the fiber, δ is the group velocity difference between the two polarization modes, β_2 represents the fiber dispersion, γ is the third-order nonlinear coefficient associated with the refractive index of the medium, and Ω_g is the gain bandwidth of the laser, which is chosen to correspond to 50 nm. The variables T and z represent time and transmission distance, respectively.

$$J(\theta, \gamma) = \begin{pmatrix} \cos\left(\frac{\gamma}{2}\right) + i\cos(2\theta)\sin\left(\frac{\gamma}{2}\right) & i\sin(2\theta)\sin\left(\frac{\gamma}{2}\right) \\ i\sin(2\theta)\sin\left(\frac{\gamma}{2}\right) & \cos\left(\frac{\gamma}{2}\right) - i\cos(2\theta)\sin\left(\frac{\gamma}{2}\right) \end{pmatrix} \quad (4)$$

The force applied to the fiber is exerted on the fiber's cross-section, specifically in the direction that forms an angle θ with the horizontal plane, resulting in the compression of the fiber. $\gamma = \delta L$, L denotes the length of the compressed fiber, which is set to 3 mm in our numerical simulations, $\delta =$

an unsaturated transmission (T_0) and modulation depth (ΔT), which is shown in the following:

$$T(I) = T_0 + (\Delta T - q(t)) \quad (1)$$

where $q(t)$ is the saturation loss of an SA, which is expressed as:

$$\frac{dq(t)}{dt} = \frac{q(t) - q_0}{\tau} - \frac{q(t)|A(t)|^2}{E_{\text{sat}}} \quad (2)$$

where q_0 is the initial absorption, τ is the recovery time, and $E_{\text{sat}} \approx 10$ pJ is the saturable absorption energy of the SA. As the intensity of the incident pulse beam increases, the transmission also increases due to saturation absorption.

Here, orthogonally polarized states are considered. Thus, the coupled nonlinear Schrödinger equation (cNLSE) describes the evolution of orthogonally polarized pulses along the EDF or SMF^[31], neglecting higher-order dispersion. The expression of the coupled NLSE is as follows:

g is the net gain of the EDF, which is only nonzero in the gain fiber section, and it is modeled as $g = g_0/(1 + E_p/E_s)$. $g_0 = 3$ is the small-signal gain coefficient, $E_s \approx 1$ nJ is the gain saturation energy of the EDF^[32-33].

The split-step Fourier method is used to solve the equations iteratively and simulate the evolution from a chirped Gaussian pulse. The mathematical model of the squeeze-typed PC is represented by the Jones matrix^[34]:

KF/d , F represents the pressure exerted on the fiber per unit length, and d represents the diameter of the compressed fiber, which is a constant value $K = 9.5 \times 10^{-5}$ rad/m.

Compared to CS, DS's formation mechanism is more complex^[35], especially for vector DS. Thus, we

plan to conduct numerical simulations of all-normal-dispersion cavities from 0.01 to 0.1 ps², as shown in Table 1.

Tab. 1 Different cavity lengths and their corresponding total net cavity dispersion

EDF L/m	SMF L/m	Entire Cavity L/m	Net Cavity Dispersion/(ps ²)
2	3	5	0.01
2.8	3	5.8	0.058
3.2	3	6.2	0.081
3.55	3	6.55	0.1

Table 1 illustrates different cavity lengths and their corresponding total net cavity dispersions. Fig. 2 (color online) depicts the corresponding output orthogonal DSs and optical spectra for various

net-normal dispersion values.

Fig. 2 shows that larger cavity dispersion leads to large pulse energy, either *X*-polarized or *Y*-polarized. However, larger cavity dispersion could cause a wide spectrum shape for the *X*-polarized and *Y*-polarized. Table 2. illustrates the output pulse parameters extracted from Fig. 2. As the net-normal dispersion increases from 0.01 ps² to 0.1 ps², the 3 dB pulse widths of *X*-polarized and *Y*-polarized pulses increase ~2.42 ps and ~1.69 ps, respectively. The 3dB spectrum widths of *X*-polarized and *Y*-polarized pulses also increase by ~2.79 nm and ~2.52 nm, respectively. This means the effect of the dispersion on pulse and spectrum widths is minimal. Thus, we chose a net cavity dispersion value of 0.01 ps² in the subsequent simulation.

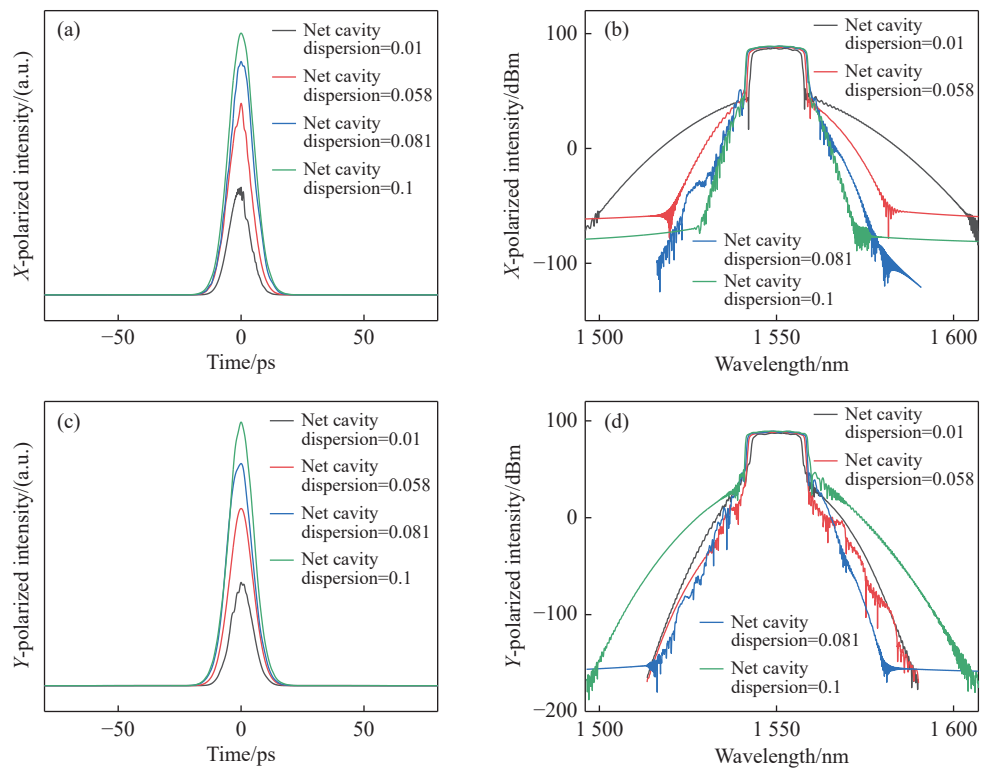


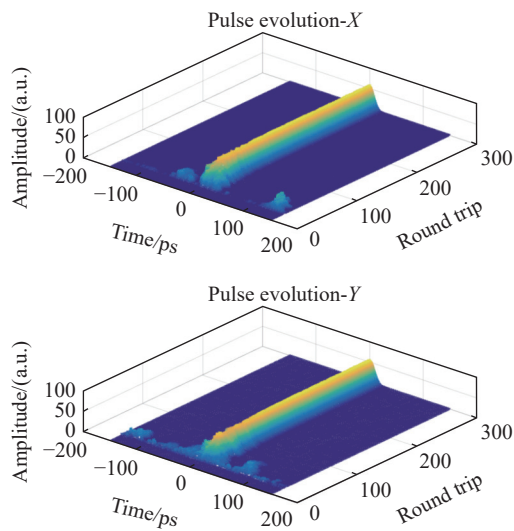
Fig. 2 Change of the output pulses and spectrum calculated with an increase of the net cavity dispersion from 0.01 ps² to 0.1 ps². (a) Output pulses of *X*-polarized. (b) Output spectrum of *X*-polarized. (c) Output pulses of *Y*-polarized. (d) Output spectrum of *Y*-polarized

Fig. 3 (color online) presents the temporal evolution of orthogonally polarized dissipative solitons within the cavity. It is observed that the pulse gradually narrows and amplifies, eventually

resulting in the output of stable orthogonally polarized dissipative solitons. The fiber laser model demonstrates excellent operational stability.

Tab. 2 The output pulse parameters associated with different cavity lengths

Net Cavity Dispersion /(ps^2)	X-polarized 3 dB pulse width/ps	Y-polarized 3 dB pulse width/ps	X-polarized 3 dB spectrum width/nm	Y-polarized 3 dB spectrum width/nm
0.01	9.52	10.18	12.34	12.15
0.058	10.43	11.2	13.83	13.94
0.081	11.17	11.69	13.04	14.06
0.1	11.94	11.87	15.13	14.67

**Fig. 3** Results from numerical simulation of orthogonally polarized dissipative soliton showing the temporal evolution of the pulse in the cavity

3 Simulation results

3.1 Effect of GMSA recovery time

Interband transition relaxation time and intraband carrier scattering and recombination relaxation time are more important parameters for our proposed GMSA, where the intraband transition relaxation time is shorter than that of the interband^[36-37]. Graphene used to fabricate SAs has many fabrication methods, such as liquid phase exfoliation, chemical vapor deposition (CVD), reduced graphene oxide (rGO), micro-mechanical cleavage, etc. Different fabrication methods could cause the differing recovery times of graphene, which can vary from hundreds of femtoseconds to a few picoseconds^[38]. The short recovery time is related to the intraband transition, while the long is caused by the interband

transition. Here, we choose recovery time ranging from 70 to 1700 fs, which is extracted from Ref [38] for covering common fabrication methods to make the GMSA.

The two polarizations' pulse width and their piecewise fitted curves are shown in Fig. 4(a) (color online). At a recovery time of 70 fs, the pulse width was found to be ~ 7.76 ps for the X-polarized and ~ 8.71 ps for the Y-polarized. Pulse widths of two polarizations gradually decrease as the recovery time increases from 70 to 120 fs. The minimum pulse width is achieved at 120 fs, where the pulse width of the X-polarized is ~ 7.47 ps and the Y-polarized is ~ 8.06 ps. When the recovery time is changed from 120 to 1700 fs, the X-polarized and Y-polarized pulse widths are increased to ~ 11.9 ps and ~ 12.0 ps, respectively. It is observed that the pulse width of the Y-polarized is consistently larger than that of the X-polarized. This is because the polarization-dependent saturable absorption of our designed GMSA leads to insufficient absorption of the Y-polarized pulse sideband energy.

Additionally, the modulation depths of our GMSA for both polarizations are calculated by changing its recovery time, as shown in Fig. 4(b) (color online). With the recovery time increase, both modulation depths increase rapidly at first and then stabilize. The modulation depth of the X-polarized and Y-polarized varies from 0.17 to 0.45 and from 0.14 to 0.4, respectively. The pulse energy and chirp versus the recovery time also have been extracted from the output pulses, as shown in Fig. 4(c)–4(d) (color online). The pulse energy range of the X-polarized varies from 3.75 to 4.63 nJ, while for the Y-polarized, it varies from 3.86 to 4.65 nJ. The variation trend of X/Y polarized pulse energies is like that of the modulation depth of two polarizations. This means the pulse energy is related to the modulation depth of the GMSA. Additionally, this is also attributed to the slow response characteristics of the mode-locked fiber laser, where pulse energy accumulation "blocks" the subsequent pulse absorption.

As a result, there is minimal absorption at the trailing edge of the pulse, which leads to an increase in pulse energy. With the increase of the recovery time, chirps for both polarizations decrease rapidly and then approach stability. Under the recovery time of 70 fs, both polarized pulses exhibit large chirp:

72 for the X -polarization and 66 for the Y -polarization. This could be attributed to the effect of the GMSA's different recovery times on the pulse shape and energy, which may alter the interaction between the dispersion and nonlinearity and subsequently affect the manifestation of the chirp.

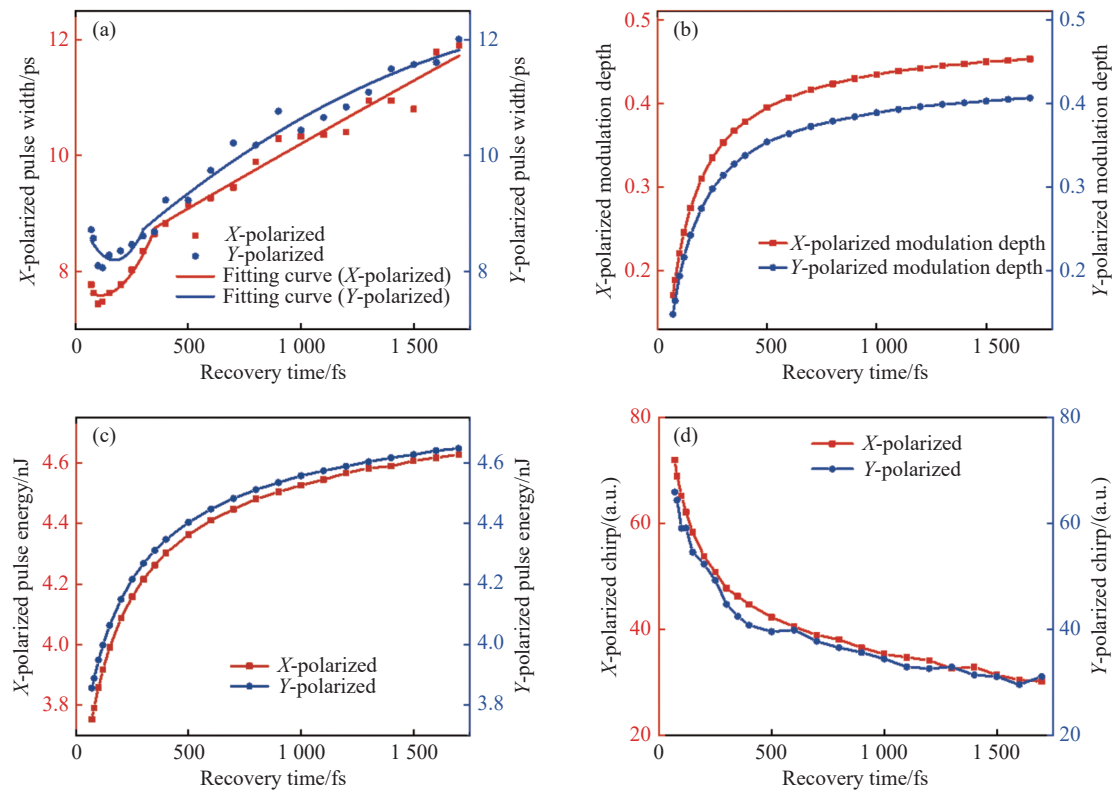


Fig. 4 (a) The influence of recovery time on the pulse width of the two orthogonal polarization components. (b) The effect of recovery time on the modulation depth for the two polarization directions. (c) The impact of recovery time on the output pulse energy of the two polarized pulses. (d) The effect of recovery time on the output pulse chirp in two polarization directions

3.2 Results analysis and discussion

To explore the function of the recovery time of our GMSA on the mode-locking pulse generation, the formation mechanisms of the mode-locking pulses are discussed in Fig. 5 (color online). Here, the recovery time of such GMSA has been divided into three stages: 70 fs, 120 fs, and 1700 fs.

(1) Recovery time equals 70 fs

Fig. 5(a) shows the compression mechanism of polarized lights by the saturable absorber when the recovery time is 70 fs. The red and blue curves represent the saturation absorption of the X -polarized

and the Y -polarized, where the initial saturation absorption of the X -polarized and the Y -polarized is fixed at 0.49 and 0.44, respectively. The modulation depth of the X -polarized and the Y -polarized are ~ 0.170 and ~ 0.147 , respectively. The output pulse width of the X -polarized ~ 7.76 ps is slightly smaller than that of the Y -polarized ~ 8.71 ps. This is due to a larger modulation depth, thus resulting in an increased absorption of the low-energy sideband of the pulse. When the recovery time of the graphene is ~ 70 fs, the light causes the intraband absorption of the graphene as a fast absorber. When the low-en-

ergy sideband of the polarized pulse enters the graphene, it can be absorbed. With the increase in sideband energy, graphene can reach deep saturation and then release within an ultra-short time of 70 fs. Subsequently, the graphene always reaches deep saturation and 70 fs release until another low-energy sideband of the polarized pulse arrives. Thus, the absorption of the central pulse energy is lower than the sideband. Furthermore, larger modulation depth leads to larger energy absorption. Thus, the energy loss of the *X*-polarized (3.75 nJ) is lower than that of the *Y*-polarized (3.86 nJ).

(2) Recovery time equals 120 fs

From Fig. 4(a), at a recovery time of 120 fs, both polarization directions reach their minimum pulse widths. This is because too fast or too slow graphene recovery time cannot effectively absorb the output pulse sideband of the mode-locking laser^[32].

In Fig. 5(b), the red curve represents the GMSA with a modulation depth of 0.245 for the *X*-polarized, while the blue curve represents the GMSA with a modulation depth of 0.216 for the *Y*-polarized. The polarization-dependent modulation depth causes different pulse widths, where a larger modulation depth leads to a smaller pulse width; a larger modulation depth also leads to larger energy loss. The *X*-polarized and *Y*-polarized pulses' energy is about 3.92 nJ and 4 nJ, respectively.

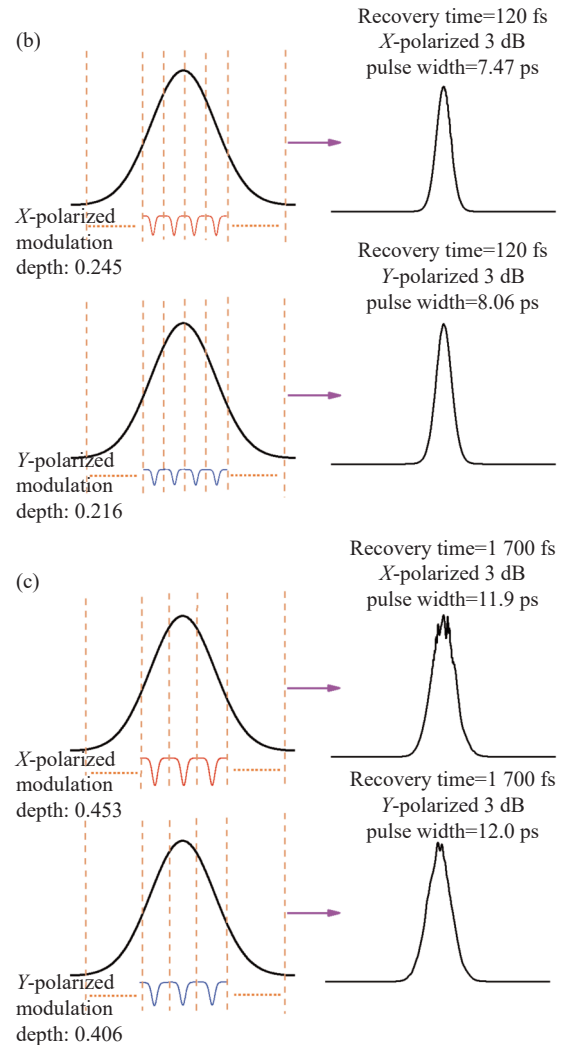
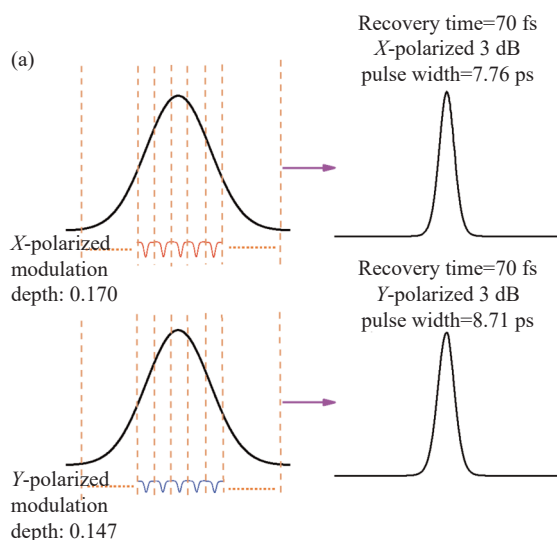


Fig. 5 Pulse formation mechanisms with different recovery times. (a) The recovery time of 70 fs. (b) The recovery time of 120 fs. (c) The recovery time of 1700 fs

(3) Recovery time equals 1700 fs

The long recovery time of 1700 fs is related to the GMSA as a slow absorber. Moreover, As shown in Fig. 5(c), a long recovery time 1700 fs leads to a significant increase in the modulation depths for both polarization directions. The modulation depth for the *X*-polarized is calculated to be ~ 0.453 , while the *Y*-polarized is ~ 0.406 . The pulse widths of the *X*-polarized and *Y*-polarized pulses are 11.9 ps and 12.0 ps, respectively. These pulse widths are larger than that of fast recovery time. When the sideband of the pulse comes into the GMSA, the long recovery time and deep modulation depth cause the pulse sideband energy to be absorbed, and

then the GMSA absorption reaches saturation. Subsequently, the GMSA should spend 1700 fs to recover. Thus, a large part of the pulse center enters the GMSA and cannot be absorbed. The overall energy of the pulse increases to broaden the pulse width. The output pulse energy for the *X*-polarized and *Y*-polarized pulses is about 4.63 and 4.65 nJ, respectively.

At a recovery time of 1700 fs, we observe the phenomenon of pulse splitting at the pulse peak. This can be attributed to the balance between nonlinearity, gain, loss, and dispersion. The fiber laser's nonlinearity is related to the pulse power and dispersion. When the output pulse energy is high, optical nonlinear effects such as self-phase modulation and cross-phase modulation could affect the pulse shape and splitting.

References:

- [1] CHANG G Q, WEI ZH Y. Ultrafast fiber lasers: an expanding versatile toolbox [J]. *iScience*, 2020, 23(5): 101101.
- [2] KIM J, SONG Y J. Ultralow-noise mode-locked fiber lasers and frequency combs: principles, status, and applications [J]. *Advances in Optics and Photonics*, 2016, 8(3): 465-540.
- [3] LI G M, YAN X H, KONG J, *et al.*. Passive mode locking in fiber lasers due to the polarization-dependent losses [J]. *Applied Optics*, 2020, 59(33): 10201-10206.
- [4] MA CH Y, GAO B, WU G, *et al.*. Observation of dissipative bright soliton and dark soliton in an all-normal dispersion fiber laser [J]. *International Journal of Optics*, 2016, 2016: 3946525.
- [5] LI X, WANG D N, HUA K, *et al.*. Saturable absorber based on graphene for a hybrid passive mode-locked erbium-doped fiber laser [J]. *Optical Fiber Technology*, 2022, 70: 102867.
- [6] TANG P H, LUO M L, ZHAO T, *et al.*. Generation of noise-like pulses and soliton rains in a graphene mode-locked erbium-doped fiber ring laser [J]. *Frontiers of Information Technology & Electronic Engineering*, 2021, 22(3): 303-311.
- [7] SALAM S, AL-MASOODI A H H, YASIN M, *et al.*. Soliton mode-locked Er-doped fiber laser by using AlQ₃ saturable absorber [J]. *Optics & Laser Technology*, 2020, 123: 105893.
- [8] HUI ZH Q, BU X F, WANG Y H, *et al.*. Bi₂O₂Te nanosheets saturable absorber-based passive mode-locked fiber laser: from soliton molecules to harmonic soliton [J]. *Advanced Optical Materials*, 2022, 10(24): 2201812.
- [9] HUANG W CH, HU L P, TANG Y F, *et al.*. Recent advances in functional 2D MXene-based nanostructures for next-generation devices [J]. *Advanced Functional Materials*, 2020, 30(49): 2005223.
- [10] WANG M K, ZI Y, ZHU J, *et al.*. Construction of super-hydrophobic PDMS@MOF@Cu mesh for reduced drag, anti-fouling and self-cleaning towards marine vehicle applications [J]. *Chemical Engineering Journal*, 2021, 417: 129265.
- [11] HUANG W CH, ZHU J, WANG M K, *et al.*. Emerging mono-elemental bismuth nanostructures: controlled synthesis and their versatile applications [J]. *Advanced Functional Materials*, 2021, 31(10): 2007584.
- [12] WANG M K, ZHU J, ZI Y, *et al.*. 3D MXene sponge: facile synthesis, excellent hydrophobicity, and high photothermal efficiency for waste oil collection and purification [J]. *ACS Applied Materials & Interfaces*, 2021, 13(39): 47302-47312.
- [13] HUANG W CH, WANG M M, HU L P, *et al.*. Recent advances in semiconducting mono-elemental selenium nanostructures for device applications [J]. *Advanced Functional Materials*, 2020, 30(42): 2003301.
- [14] HUANG W CH, ZHANG Y, YOU Q, *et al.*. Enhanced photodetection properties of tellurium@selenium roll-to-roll

4 Conclusion

An orthogonally polarized numerical modeling of the PML graphene fiber laser with a net-normal dispersion birefringent cavity has been established. The output of orthogonally polarized pulses with different normal net cavity dispersion has been discussed. The influence of the recovery time of the GMSA on the mode-locking performance is investigated by utilizing our modeling. It is found that the recovery time significantly affects the pulse characteristics of two orthogonally polarized pulses. GMSA with a recovery time of 120 fs could help to generate narrow dissipative soliton pulses with large chirps for two orthogonally polarized directions, about 7.47 ps and 8.06 ps.

- nanotube heterojunctions[J]. *Small*, 2019, 15(23): 1900902.
- [15] KIM D, PARK N H, LEE H, *et al.*. Graphene-based saturable absorber and mode-locked laser behaviors under gamma-ray radiation[J]. *Photonics Research*, 2019, 7(7): 742-747.
- [16] SUN ZH P, HASAN T, TORRISI F, *et al.*. Graphene mode-locked ultrafast laser[J]. *ACS Nano*, 2010, 4(2): 803-810.
- [17] CAO T, LIU SH ZH, GUO Z Y, *et al.*. Quantification of dissipative effects in a complex Ginzburg-Landau equation governed laser system by tracing soliton dynamics[J]. *Opt Express*, 2023, 31(3): 4055-4066.
- [18] CABASSE A, ORTAÇ B, MARTEL G, *et al.*. Dissipative solitons in a passively mode-lock Er-doped fiber with strong normal dispersion[J]. *Optics Express*, 2008, 16(23): 19322-19329.
- [19] SONG Y F, SHI X J, WU CH F, *et al.*. Recent progress of study on optical solitons in fiber lasers[J]. *Applied Physics Reviews*, 2019, 6(2): 021313.
- [20] LIU X J, HU P, LIU Y, *et al.*. Conventional solitons and bound-state solitons in an erbium-doped fiber laser mode-locked by TiSe₂-based saturable absorber[J]. *Nanotechnology*, 2020, 31(36): 365202.
- [21] ZHANG H, TANG D Y, ZHAO L M, *et al.*. Vector dissipative solitons in graphene mode locked fiber lasers[J]. *Optics Communications*, 2010, 283(17): 3334-3338.
- [22] DUDLEY J M, DIAS F, ERKINTALO M, *et al.*. Instabilities, breathers and rogue waves in optics[J]. *Nature Photonics*, 2014, 8(10): 755-764.
- [23] LECAPLAIN C, GRELU P, SOTO-CRESPO J M, *et al.*. Dissipative rogue waves generated by chaotic pulse bunching in a mode-locked laser[J]. *Physical Review Letters*, 2012, 108(23): 233901.
- [24] RENNINGER W H, CHONG A, WISE F W. Dissipative solitons in normal-dispersion fiber lasers[J]. *Physical Review A*, 2008, 77(2): 023814.
- [25] LAN H W, CHEN F L, WANG Y T, *et al.*. Polarization dynamics of vector solitons in a fiber laser[J]. *Optics Express*, 2023, 31(13): 21452-21463.
- [26] LEE J, KWON S, ZHAO L M, *et al.*. Investigation into the impact of the recovery time of a saturable absorber for stable dissipative soliton generation in Yb-doped fiber lasers[J]. *Optics Express*, 2021, 29(14): 21978-21991.
- [27] XU SH T, TURNALI A, SANDER M Y. Group-velocity-locked vector solitons and dissipative solitons in a single fiber laser with net-anomalous dispersion[J]. *Scientific Reports*, 2022, 12(1): 6841.
- [28] ZHAO L M. *Vector Dissipative Solitons*[M]//FERREIRA M F S. Dissipative Optical Solitons. Cham: Springer, 2022: 105-130.
- [29] YAN R B, HE X Y, ZHANG CH, *et al.*. SSFM-global-error-local-energy method for improving computational efficiency of passively mode-locked fiber laser[J]. *Chinese Optics*, 2023, 16(3): 733-742. (in Chinese).
- [30] HE X Y, WANG D N, LIU ZH B. Pulse-width tuning in a passively mode-locked fiber laser with graphene saturable absorber[J]. *IEEE Photonics Technology Letters*, 2014, 26(4): 360-363.
- [31] LIU X M. Pulse evolution without wave breaking in a strongly dissipative-dispersive laser system[J]. *Physical Review A*, 2010, 81(5): 053819.
- [32] LEE J, KWON S, LEE J H. Numerical investigation of the impact of the saturable absorber recovery time on the mode-locking performance of fiber lasers[J]. *Journal of Lightwave Technology*, 2020, 38(15): 4124-4132.
- [33] LI D J, TANG D Y, ZHAO L M, *et al.*. Mechanism of dissipative-soliton-resonance generation in passively mode-locked all-normal-dispersion fiber lasers[J]. *Journal of Lightwave Technology*, 2015, 33(18): 3781-3787.
- [34] QIN T. *The development of the electric PZT extrude fiber polarization controller*[D]. Beijing: Beijing Jiaotong University, 2014. (in Chinese).
- [35] HAN D D, ZHANG J Y, REN K L, *et al.*. Real-time measurement of fission dynamics of dissipative soliton[J]. *Acta Optica Sinica*, 2022, 42(7): 0706001. (in Chinese).
- [36] DAWLATY J M, SHIVARAMAN S, CHANDRASHEKHAR M, *et al.*. Measurement of ultrafast carrier dynamics in epitaxial graphene[J]. *Applied Physics Letters*, 2008, 92(4): 042116.
- [37] BREUSING M, ROPERS C, ELSAESSER T. Ultrafast carrier dynamics in graphite[J]. *Physical Review Letters*, 2009, 102(8): 086809.
- [38] SUN Z, HASAN T, FERRARI A C. Ultrafast lasers mode-locked by nanotubes and graphene[J]. *Physica E: Low-dimensional Systems and Nanostructures*, 2012, 44(6): 1082-1091.

Author Biographics:



He Xiao-ying (1981—), female, born in Jingzhou, Hubei. She received her Ph.D. degree from the Huazhong University of Science and Technology in 2009. She now works as an associated investigator at the Beijing University of Posts and Telecommunications. Her main research interests include semiconductor optoelectronic devices, neural synaptic devices, fiber mode-locking lasers, and beam shaping. E-mail: xiaoyinghe@bupt.edu.cn

《中国光学(中英文)》征稿启事

《中国光学(中英文)》为双月刊, A4 开本; 刊号: ISSN 2097-1842/CN 22-1431/04; 国内外公开发行, 邮发代号: 国内 12-140, 国外 BM6782。

- | | |
|-----------------|----------------|
| ★ 荷兰 Scopus 数据库 | ★ 中国精品科技期刊 |
| ★ 美国《乌利希国际期刊指南》 | ★ 中国科技核心期刊 |
| ★ 美国《化学文献》 | ★ 中国光学学会会刊 |
| ★ 波兰《哥白尼索引》 | ★ 中国科技论文与引文数据库 |
| ★ 俄罗斯《文摘杂志》 | ★ 中国期刊全文数据库 |
| ★ 美国工程索引(Ei)数据库 | ★ 万方数字化期刊全文数据库 |
| ★ 美国 ESCI 数据库 | ★ 中国科技期刊数据库 |
| | ★ 中国光学期刊网数据库 |

主要栏目:微纳光学、信息光学、集成光电子、光谱学和光谱仪器、激光技术与应用、光学功能材料、光学设计与工艺、大气与空间光学、光学仪器与测试、综述、前沿动态、产业资讯、科普教学、实验室介绍、自然科学基金项目进展、前沿热点访谈、热点论文等。

发稿类型:学术价值显著、实验数据完整的原创性论文; 研究前景广阔, 具有实用、推广价值的技术报告; 有创新意识, 能够反映当前先进水平的阶段性研究简报; 对当前学科领域的研究热点和前沿问题的专题报告; 以及综合评述国内外光学技术研究现状、发展动态和未来发展趋势的综述性论文。

欢迎投稿、荐稿。

主管单位: 中国科学院

主办单位: 中国科学院长春光学精密机械与物理研究所

协办单位: 激光与物质相互作用国家重点实验室

编辑出版: 《中国光学(中英文)》编辑部

投稿网址: <http://chineseoptics.net.cn>

邮件地址: chineseoptics@ciomp.ac.cn

联系电话: 0431-84627061

传 真: 0431-84627061

编辑部地址: 长春市东南湖大路 3888 号(130033)